Controlled Synthesis of Compositionally Tunable Ternary $PbSe_xS_{1-x}$ as Well as Binary PbSe and PbS Nanowires

Anthony C. Onicha,[†,§] Nattasamon Petchsang,[†,§] Thomas H. Kosel,[‡] and Masaru Kuno[†,*]

[†]Department of Chemistry and Biochemistry, and [‡]Department of Electrical Engineering, University of Notre Dame, Notre Dame, Indiana 46556, United States.
[§]These authors contributed equally to the study.

ABSTRACT

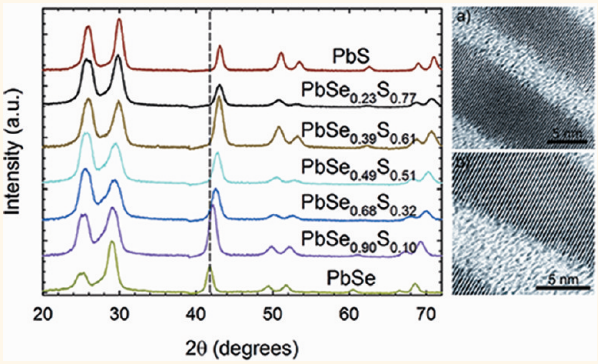

High-quality compositionally tunable ternary $PbSe_xS_{1-x}$ (x = 0.23, 0.39, 0.49, 0.68, and 0.90) nanowires (NWs) and their binary analogues have been grown using solution–liquid–solid growth with lead(II) diethyldithiocarbamate, $Pb(S_2CNEt_2)_2$, and lead(II) imido(bis(selenodiisopropylphosphinate)), $Pb((SeP^iPr_2)_2N)_2$, as single-source precursors. The alloyed nature of $PbSe_xS_{1-x}$ wires was confirmed using ensemble X-ray diffraction and energy dispersive X-ray spectroscopy (EDXS). Single NW EDXS line scans taken along the length of individual wires show no compositional gradients. NW compositions were independently confirmed using inductively coupled plasma atomic emission spectroscopy. Slight stoichiometric deviations occur but never exceed 13.3% of the expected composition, based on the amount of introduced precursor. In all cases, resulting nanowires have been characterized using transmission electron microscopy. Mean diameters are between 9 and 15 nm with accompanying lengths that range from 4 to 10 μm. Associated selected area electron diffraction patterns indicate that the $PbSe_xS_{1-x}$, PbSe, and PbS NWs all possess the same ⟨002⟩ growth direction, with diffraction patterns consistent with an underlying rock salt crystal structure.

KEYWORDS: single-source precursor · solution–liquid–solid growth · nanowire · lead selenide · lead sulfide · lead selenide sulfide · binary · ternary · solid solution · alloy

Lead chalcogenide nanostructures have attracted significant interest due to their potential use in sensors,[1,2] solar photovoltaics,[3,4] infrared photodetectors,[5,6] and thermoelectric devices.[7,8] In many cases, this stems from their narrow band gaps (PbS = 0.41 eV,[9] PbSe = 0.28 eV,[9] PbTe = 0.23 eV[10]) and large bulk exciton Bohr radii (PbS = 18 nm,[3] PbSe = 46 nm,[11] PbTe = 150 nm[3]). Though controversial, multiple exciton generation has been demonstrated in PbSe and PbS nanocrystals (NCs) and could eventually aid the development of more efficient solar photovoltaics.[12,13] Nanowires (NWs) offer advantages over nanocrystals in such applications. They include anisotropic shapes that allow for improved carrier mobilities,[14] absorption/emission polarization sensitivities,[15,16] and larger absorption cross sections as compared to NCs.[14]

Common techniques for growing lead chalcogenide NWs include chemical vapor deposition (CVD),[8,17–19] template-based growth,[20,21] epitaxial growth,[22] and solution-based approaches.[23–29] Reported solution-phase syntheses of PbSe and PbS NWs include solvothermal growth,[28] the oriented attachment of nanoparticles,[26,27,29] and solution–liquid–solid (SLS) growth.[23–25] In the latter, SLS approach, metal/chalcogen precursor pairs such as lead acetate/trioctylphosphine selenide (TOPSe)[25] and lead oleate/trioctylphosphine sulfide (TOPS)[23] have been explored to produce PbSe and PbS NWs. Recently, Sun *et al.*[24] have reported the use of lead(II) diethyldithiocarbamate, $Pb(S_2CNEt_2)_2$, as a single-source precursor for the SLS growth of high-quality PbS NWs. Details of the mechanism underpinning SLS growth can be found in the literature.[30,31]

Although single-source precursors have been extensively developed for the metal–organic chemical vapor deposition (MOCVD) of semiconductor thin films,[32] only a handful of publications have reported their successful use in SLS preparations.[24,33,34] One advantage of single-source precursors involves having both metal and chalcogen elements in close proximity. This ameliorates growth issues stemming from the different decomposition kinetics and/or reactivities of separate

* Address correspondence to mkuno@nd.edu.

Received for review January 25, 2012 and accepted February 16, 2012.

Published online February 16, 2012
10.1021/nn300373w

metal/chalcogen precursors. While the mechanism behind the decomposition of these single-source precursors is not fully understood, their use empirically results in the growth of homogeneous nanowires.

With this in mind, the growth of compositionally complex nanostructures such as ternary alloys remains a great challenge in current nanoscience. This is true even in nanocrystals, where it has been difficult to find precursors for constituent elements that result in equal growth rates and whose optimal growth conditions do not impede each other.[35] Among reasons for creating ternary alloys is the opportunity to achieve band gap tuning by varying the material's composition rather than size. This gives researchers access to a new class of nanomaterials, possessing both size- and composition-dependent optical/electrical properties. Ternary growth has been demonstrated in $Zn_xCd_{1-x}S$ (x = 0.10, 0.25, 0.36, 0.53),[36] $Zn_xCd_{1-x}Se$ (x = 0.28, 0.44, 0.55, 0.67),[37] CdS_xSe_{1-x} (x = 0.13, 0.34, 0.53, 0.76),[38] $CdSe_{1-x}Te_x$ (x = 0.39, 0.66, 0.85),[39] and PbS_xSe_{1-x} {x = (0.35, 0.50, 0.70, 0.95),[3] (0.20, 0.33, 0.43, 0.50, 0.67, 0.80),[35] (0.11, 0.26, 0.54, 0.77, 0.86)[40]} nanocrystals with resulting band gaps tunable between those of their respective binary systems.

Despite these initial successes, the available literature on solution-grown ternary NCs indicates that even in these 0D systems, the constituent elements are not homogenously alloyed.[3,35] Although no phase separation has been reported, the available literature does indicate some degree of segregation with one of the elements accumulating off-center. This results in radial heterogeneities.[3,35] The synthesis of ternary NWs represents an even greater challenge since one must maintain not only radial but also compositional homogeneity across the NW length. The growth of single-crystalline ternary NWs has been reported for $CuInSe_2$ (Cu/In/Se = 33:22:45; 46:18:36),[33] $Cu_{2-x}S_ySe_{1-y}$ (Cu/S/Se = 62:38:0, 61:28:11, 61:20:19, 61:15:24, 62:10:28, 62:0:38),[41] $In_xGa_{1-x}N$ (x = 0−1),[42] ZnS_xSe_{1-x} (x = 0.21, 0.35, 0.49, 0.60, 0.71, 0.80),[43] and $ZnSe_xTe_{1-x}$ (compositional gradient with Se:Te = 3.9:1, 2.7:1, 1.4:1, 1:1 along the length of a wire).[44] Furthermore, although these NWs exhibit no phase segregation, longitudinal compositional variations exist in all cases where a detailed compositional analysis has been carried out.[33,42,44] Furthermore, ternary $PbSe_xS_{1-x}$ NWs (x = 0.40) have been reported by Mokari *et al.*[45] using lead oleate/trioctylphosphine sulfide as precursors.

In the present study, we report the use of lead(II) imido(bis(selenodiisopropylphosphinate)), $Pb((SeP^iPr_2)_2N)_2$, and lead(II) diethyldithiocarbamate, $Pb(S_2CNEt_2)_2$, as single-source precursors for the growth of ternary $PbSe_xS_{1-x}$ (where x = 0.23, 0.39, 0.49, 0.68, 0.90) as well as binary PbSe and PbS NWs. Resulting wires have been characterized using transmission electron microscopy (TEM), scanning transmission electron microscopy (STEM), energy dispersive X-ray spectroscopy (EDXS), X-ray diffraction (XRD), and elemental analysis through inductively coupled plasma atomic emission spectroscopy (ICP-AES). Binary nanowires possess mean diameters between 9 and 15 nm, while ternary wires are approximately 10 nm in diameter. Accompanying NW lengths range from 4 to 10 μm. In $PbSe_xS_{1-x}$, more detailed single-NW EDXS analyses reveal slight compositional inhomogeneities (with 6.83 $\pm$ 0.03% variations) along the growth direction. ICP-AES elemental analyses also show analogous deviations for both binary and ternary NW ensembles though never exceeding 13.3% of the intended composition, based on the amount of introduced precursor. The current synthesis therefore effectively produces compositionally tunable ternary NWs with no evidence of composition gradients. This points to the successful implementation of single-source precursors in producing compositionally complex nanowires.

RESULTS AND DISCUSSION

The use of single-source precursors in the synthesis of metal chalcogenide nanowires provides a unique opportunity to eliminate the problem of empirically finding separate metal and chalcogen sources that possess appropriately balanced reactivities.[24] Since both the metal and chalcogen exist on the same compound, this suppresses any variabilities in precursor decomposition kinetics that can adversely affect NW growth. More importantly, the use of single-source precursors aids the growth of compositionally complex ternary nanowires where finding appropriate metal and chalcogen precursors, with comparable decomposition kinetics and growth compatibilities, can be difficult or even prohibitive.

To ascertain the feasibility of using single-source precursors for the seeded growth of ternary $PbSe_xS_{1-x}$ NWs, we first employed these compounds to grow binary PbSe and PbS wires. Their growth was optimized by varying parameters such as the coordinating/noncoordinating nature of the growth solvent, the reaction temperature, and the amount of Bi catalyst introduced.[46,47] In all cases, single-source precursors were recrystallized prior to use. Growth solvents such as trioctylphosphine oxide (TOPO), trioctylphosphine (TOP), hexadecylamine (HDA), octadecene, and squalane were investigated, the details of which are presented in the Supporting Information (Table S1). Empirically, the highest quality NWs, in terms of their surface smoothness, straightness, diameter, and length, were grown using TOPO. For all NWs reported and for the same amount of catalyst, growth temperatures of T > 230 °C led to thick ($d \approx$ 20 nm) NWs, with diameters decreasing with decreasing temperature. Below 200 °C, large-diameter wires were again observed. Since both single-source precursors led to PbSe and PbS NWs with similar diameters at

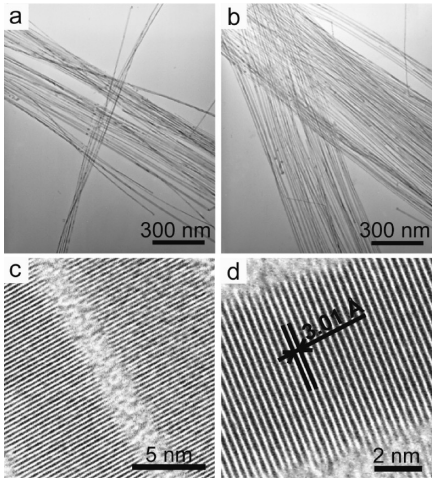

Figure 1. (a, b) Low- and (c, d) high-resolution TEM images of PbSe NWs with a mean diameter of $d = 9 \pm 2$ nm (±21%).

T = 210 °C, this temperature was selected as our default growth temperature.

Figure 1 shows representative low- and high-resolution TEM images of the PbSe NWs produced. Clear lattice fringes are evident, illustrating their crystallinity. The wires also have smooth surfaces and exhibit straight morphologies, as opposed to the branched shapes previously seen in solution-grown II–VI[48,49] and IV–VI NWs.[25]

For the PbSe ensemble shown, NWs possess a mean diameter of 9 ± 2 nm (±21%, sample size 24 NWs). Lengths exceed 10 μm with corresponding intrawire diameter variations of ±8%. By varying the amount of introduced $BiCl_3$ while maintaining the amount of added $Pb((SeP^iPr_2)_2N)_2$ constant at 20 μmol, the following PbSe nanowire diameters could be obtained: (a) 25 nmol of $BiCl_3$ [d = 9 ± 1 nm (±11%, sample size 30 NWs), associated $BiCl_3$:$Pb((SeP^iPr_2)_2N)_2$ ratio = 1:784], (b) 50 nmol of $BiCl_3$ [d = 11 ± 2 nm (±18%, sample size 30 NWs), associated $BiCl_3$:$Pb((SeP^iPr_2)_2N)_2$ ratio = 1:392], (c) 100 nmol of $BiCl_3$ [d = 13 ± 2 nm (±15%, sample size 40 NWs), associated $BiCl_3$:$Pb((SeP^iPr_2)_2N)_2$ ratio = 1:196], (d) 200 nmol of $BiCl_3$ [d = 15 ± 2 nm (±13%), sample size 30 NWs, associated $BiCl_3$:$Pb((SeP^iPr_2)_2N)_2$ ratio = 1:98]. This diameter dependence is consistent with our earlier observations on CdSe NWs where introducing more $BiCl_3$ led to larger Bi nanoparticles, which, in turn, resulted in larger diameter NWs.[50] Additional TEM images of PbSe NWs, showing clear lattice fringes and smooth surfaces, can be found in the Supporting Information (Figure S1).

Figure 2 shows representative TEM images of analogous d = 9 ± 2 nm (±22%, sample size 69 NWs) PbS NWs produced under similar conditions. As with PbSe, the wires exhibit smooth surfaces and straight morphologies. The accompanying high-resolution images also show that the wires are crystalline. An analogous diameter dependence with the amount of introduced

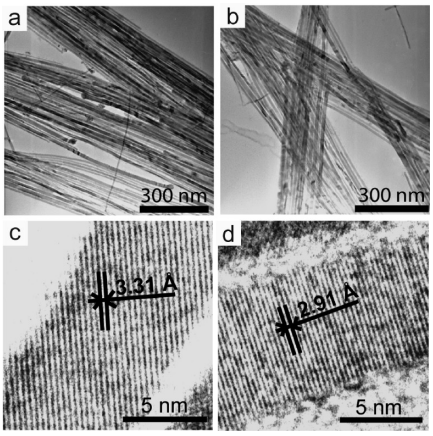

Figure 2. (a, b) Low- and (c, d) high-resolution TEM images of PbS NWs with a mean diameter of $d = 9 \pm 2$ nm (±22%).

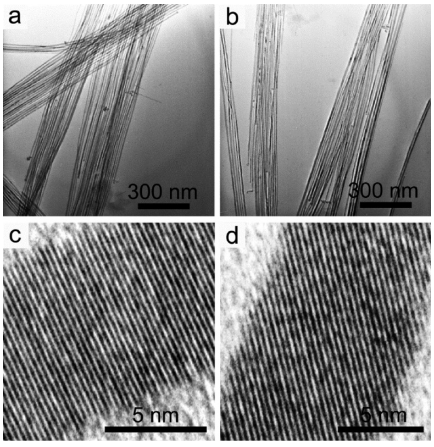

Figure 3. (a, b) Low- and (c, d) high-resolution TEM images of $PbSe_{0.50}S_{0.50}$ NWs with a mean diameter of $d = 10 \pm 2$ nm (±20%).

$BiCl_3$ is observed. Additional TEM images of PbS NWs showing straight morphologies, smooth surfaces, and clear lattice fringes can be found in the Supporting Information (Figures S2 and S3).

Having confirmed the feasibility of using single-source precursors to grow PbSe and PbS NWs, we proceeded to tackle the synthesis of compositionally tunable $PbSe_xS_{1-x}$ NWs. Procedures for making PbSe and PbS NWs were therefore modified by mixing both $Pb((SeP^iPr_2)_2N)_2$ and $Pb(S_2CNEt_2)_2$ precursors in subsequent reactions. The composition of resulting ternary NWs was controlled by introducing the $Pb((SeP^iPr_2)_2N)_2$:$Pb(S_2CNEt_2)_2$ mole ratios 4:1, 1.5:1, 1:1, 1:1.5, and 1:4 to obtain $PbSe_{0.80}S_{0.20}$, $PbSe_{0.60}S_{0.40}$, $PbSe_{0.50}S_{0.50}$, $PbSe_{0.40}S_{0.60}$, and $PbSe_{0.20}S_{0.80}$ NWs, respectively. In all cases, the amount of introduced $BiCl_3$ was kept constant at 1.25 nmol per 1.0 μmol of total precursor [*i.e.*, both $Pb((SeP^iPr_2)_2N)_2$ and $Pb(S_2CNEt_2)_2$] to maintain a mean NW diameter of approximately 10 nm. In what follows, we refer to the different ternary ensembles through their theoretical stoichiometries.

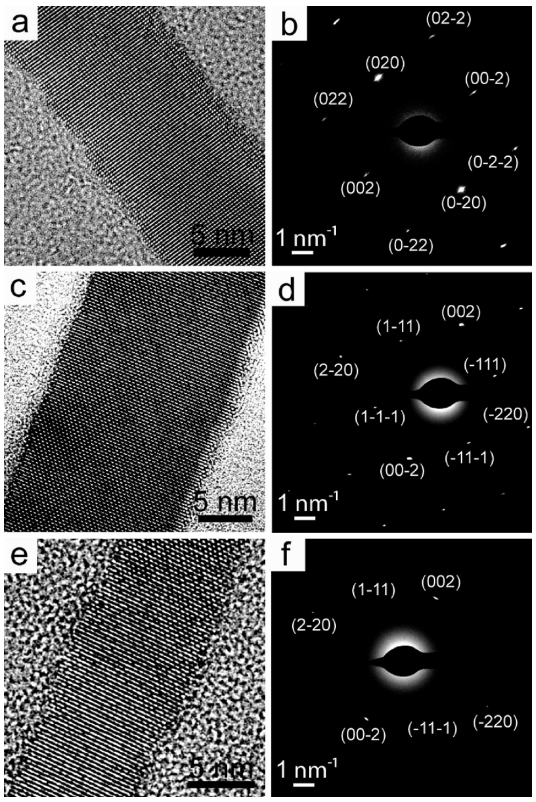

Figure 4. High-resolution TEM images and corresponding SAED patterns for (a, b) PbSe, (c, d) PbS, and (e, f) $PbSe_{0.50}S_{0.50}$ NWs.

Figure 3 shows representative low- and high-resolution TEM images of $PbSe_{0.50}S_{0.50}$ NWs produced. The sample's mean diameter is $d = 10 \pm 2$ nm (±20%, sample size 45 NWs) with the following (mean) diameters for other preparations: $PbSe_{0.80}S_{0.20}$, 11 ± 3 nm (±27%, sample size 30 NWs); $PbSe_{0.60}S_{0.40}$, 9 ± 2 nm (±22%, sample size 45 NWs); $PbSe_{0.40}S_{0.60}$, 9 ± 1 nm (±11%, sample size 40 NWs); and $PbSe_{0.20}S_{0.80}$, 9 ± 2 nm (±22%, sample size 30 NWs). In all cases, corresponding intrawire diameter variations are less than ±11%.

Representative high-resolution TEM micrographs and corresponding selected area electron diffraction (SAED) patterns of PbSe, PbS, and $PbSe_{0.50}S_{0.50}$ NWs are shown side-by-side in Figure 4. In all cases, the diffraction patterns are consistent with a face-centered cubic structure,[51] with the observed spot pattern depending on the zone axis being viewed. To illustrate, the SAED pattern in Figure 4b corresponds to viewing the NW down the ⟨100⟩ zone. The pattern in Figure 4d results from probing the ⟨110⟩ zone axis. Contributing planes in all SAED patterns have been indexed and are {002}, {111}, and {220}. The brightest spots lie along the NW long axis and determine its growth direction. Figure 4b therefore shows a [020] growth direction, while Figure 4d and 4f illustrate a [002] growth direction; both are identical in the cubic NW lattice. Together these SAED images reveal that both binary and ternary NWs possess ⟨002⟩ growth axes.

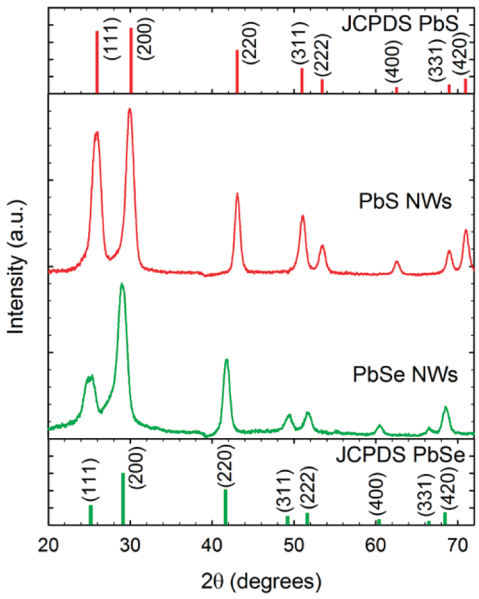

Figure 5. XRD patterns of PbS and PbSe NWs along with their corresponding JCPDS reflections. Traces are offset for clarity.

This conclusion was further corroborated by measuring the TEM lattice fringe spacing of binary NWs viewed along ⟨100⟩ (Figures 1c, 1d, 2d, 3c) and ⟨110⟩ (Figures 2c and 3d). For PbSe NWs viewed along ⟨100⟩ we measure a {002} fringe spacing of 3.01 Å. The corresponding database value is 3.06 Å (JCPDS 77-0245). For PbS we measure a 2.91 Å {002} fringe spacing. This agrees well with its 2.92 Å database value (JCPDS 77-0244). For PbSe and PbS wires viewed along ⟨110⟩, their {111} *d*-spacings likewise agree with their database values (PbSe: 3.45 Å experimental *versus* 3.53 Å database value; PbS: 3.31 Å experimental *versus* 3.42 Å database value). These results confirm that produced binary NWs grow along ⟨002⟩. Furthermore, both the SAED and *d*-spacing measurements corroborate growth direction conclusions from earlier PbS[24] and PbSe[25] NW reports.

PbSe and PbS NW crystal structures were further characterized using ensemble XRD measurements. Figure 5 shows resulting data for representative PbSe and PbS ensembles along with their respective JCPDS stick patterns. The positions and relative intensities of the PbSe/PbS reflections agree with their database values [PbSe: JCPDS 77-0245 (a = 6.128 Å); PbS: JCPDS 77-0244 (a = 5.934 Å)]. This indicates that they exhibit the rock salt crystal structure. Differences in the experimental peak intensities relative to their JCPDS values however arise due to crystallographic texture.[52] This is because the angles of incidence and reflection are equal in the XRD experiment. As a consequence, observable reflections arise only from crystal planes parallel to the specimen substrate.[53]

Figure 6 compares the XRD patterns of $PbSe_xS_{1-x}$ NWs to their binary counterparts. It is apparent that the

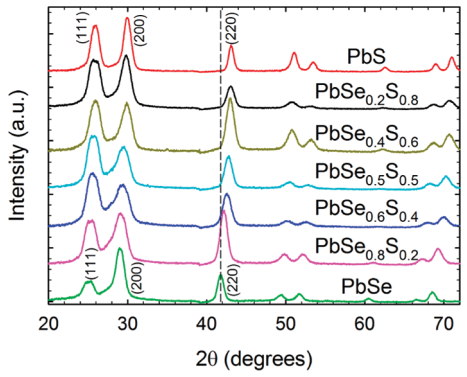

Figure 6. XRD patterns of ternary NWs with corresponding PbSe and PbS reflections for comparison purposes. The dashed line is a guide to the eye. Traces are offset for clarity.

ternary wires exhibit the same overall reflection pattern as their parent PbSe and PbS NWs. This indicates that the $PbSe_xS_{1-x}$ NWs retain an identical rock salt crystal structure. Figure 6 also shows that they exhibit reflections that lie between the corresponding binary PbSe/PbS NW reflections and that shift with increasing sulfur content. To illustrate, the (220) PbSe reflection occurs at 41.7°. It moves to 42.7° in $PbSe_{0.5}S_{0.5}$ and settles at 43.1° in PbS. A dashed line has been included in Figure 6 to guide the eye. Similar behavior can be seen with the other reflections. A plot illustrating this can be found in the Supporting Information (Figure S4).

Another way to visualize these reflection angle shifts is to extract the lattice constant associated with each XRD pattern. For this purpose, we used Bragg's law to calculate the composition-dependent *a*-values of $PbSe_xS_{1-x}$ NWs. Namely, $2d_{hkl}\sin(\theta) = n\lambda$ was used to determine d_{hkl}, which subsequently yielded *a* through $d_{hkl} = a/(h^2 + k^2 + l^2)^{1/2}$. In the equations, d_{hkl} is the *d*-spacing associated with a given (*hkl*), θ is the angle between the incident X-ray beam and the crystal plane, *n* is the order of the reflection (usually $n = 1$), λ is the X-ray wavelength (1.54 Å), *a* is the desired lattice constant, and *h, k, l* are Miller indices. In all samples, an average *a*-value was obtained by carrying out the calculation on the (220), (311), (222), (400), (331), and (420) reflections (Figure 6). Smaller angle reflections [i.e., (111) and (200)] were not used since substrate-related contributions to the background were found to introduce significant errors. For comparison purposes, the parent binary compound lattice constants were also calculated. We obtain for PbSe 6.117 Å measured *versus* 6.128 Å database value and for PbS 5.931 Å measured *versus* 5.934 Å database value. Both pairs of values are therefore self-consistent.

Corresponding ternary NW lattice constants lie between the above PbSe/PbS limits and shift with composition. This indicates their ternary nature. $PbSe_xS_{1-x}$ *a*-values are summarized in Table 1.

TABLE 1. Calculated Lattice Constants of PbSe, PbS, and $PbSe_xS_{1-x}$ NWs from an Analysis of Ensemble XRD Patterns and Estimated Compositions Based on Ensemble EDXS and ICP-AES Measurements

		ensemble EDXS results		ensemble ICP-AES results	
	XRD results				
nominal composition	*a* (Å)	*x*	1−*x*	*x*	1−*x*
PbS	5.931 ± 0.002				
$PbSe_{0.20}S_{0.80}$	5.954 ± 0.010	0.18	0.82	0.23 (±0.014)	0.77 (±0.014)
$PbSe_{0.40}S_{0.60}$	5.956 ± 0.006	0.27	0.73	0.39 (±0.014)	0.61 (±0.014)
$PbSe_{0.50}S_{0.50}$	5.989 ± 0.010	0.43	0.57	0.49 (±0.021)	0.51 (±0.021)
$PbSe_{0.60}S_{0.40}$	6.013 ± 0.012	0.52	0.48	0.68 (±0.014)	0.32 (±0.014)
$PbSe_{0.80}S_{0.20}$	6.062 ± 0.005	0.73	0.27	0.90 (±0.014)	0.10 (±0.014)
PbSe	6.117 ± 0.003				

We investigated whether binary and ternary NWs conformed to Vegard's law.[54] Namely, Vegard's law states that $a_{\text{ternary NWs}} = xa_{PbSe} + (1 - x)a_{PbS}$, where *x* is the mole fraction of the introduced substituent, and $a_{\text{ternary NWs}}$, a_{PbSe}, and a_{PbS} are the lattice constants of $PbSe_xS_{1-x}$, PbSe, and PbS, respectively. Lattice constants, calculated from our XRD results, were therefore plotted as a function of composition (*x*), using ensemble ICP-AES-derived stoichiometries (see Supporting Information Figure S5). What results is a nonlinear "bowing" of *a* with *x*, indicating a departure from Vegard's law. Such deviations are not unusual, and bowing has previously been seen in ternary CdS_xSe_{1-x},[38] $CdSe_xTe_{1-x}$,[39] and $PbSe_xS_{1-x}$[35] NCs. Detailed theoretical calculations attribute this nonlinearity to the lattice constant mismatch of the parent compounds as well as their different atomic sizes and electronegativities.[55−57] Alternatively, deviations can arise from internal stresses arising from surface ligands, which can alter nanostructure lattice parameters.[56,58,59] The predicted Vegard's law linear relationship is therefore only a first-order approximation, and in some semiconductor systems a modified quadratic equation is invoked to accurately describe the observed lattice constant or band gap dependence with composition.[35,43,60]

Two approaches were undertaken to ascertain the NW stoichiometry. First, EDXS measurements of small PbSe, PbS, and $PbSe_xS_{1-x}$ NW ensembles (sample size ~30 NWs for each NW sample) were undertaken to estimate their composition. These measurements show that binary PbSe NWs possess an approximate 1:1 metal-to-chalcogen ratio (Pb:Se = 54%:46%). A representative spectrum can be found in the Supporting Information (Figure S6). EDXS compositional analyses of PbS and $PbSe_xS_{1-x}$ nanowires, however, were complicated by the spectral overlap of the sulfur K and lead M lines. To partially address this issue,

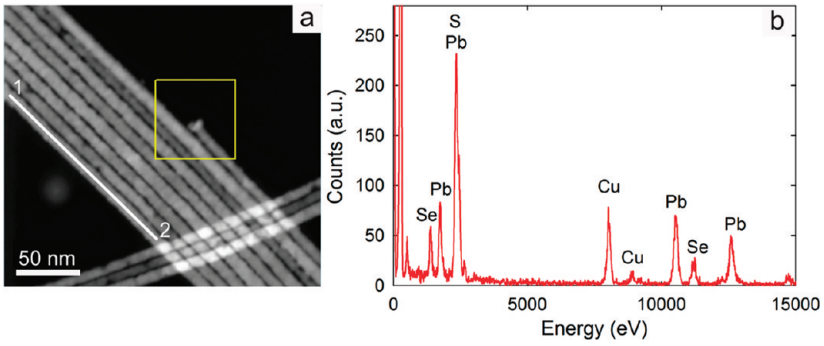

Figure 7. (a) Representative HAADF–STEM image of a small $PbSe_{0.60}S_{0.40}$ NW bundle. The boxed region represents a reference area used for an automated TEM drift correction procedure. (b) Single-NW EDXS spectrum collected along the white line in (a) from points 1 to 2. A total of 10 spectra were acquired along the line profile.

ternary NW compositions were therefore assessed using a Cliff–Lorimer analysis,[61] the details of which are presented in the Supporting Information. Results of these EDXS calculations are listed in Table 1.

To further verify ternary NW stoichiometries and to avoid issues with the S/Pb spectral overlap, ensemble ICP-AES measurements were used to determine the compositions of NW ensembles, the synthesized single-source precursors, and commercial PbSe and PbS standards. Results of this analysis show that binary PbSe (Pb:Se = 0.51:0.49) and PbS (Pb:S = 0.54:0.46) NWs have an approximate 1:1 metal-to-chalcogen ratio. Likewise, commercial PbSe and PbS standards show a 1:1 metal-to-chalcogen ratio, and the $Pb(S_2CNEt_2)_2$ and $Pb((SeP^iPr_2)_2N)_2$ single-source precursors exhibit their expected 1:4 lead-to-chalcogen ratios.

For ternary NWs, ICP-AES results reveal the following compositions: $PbSe_{0.23}S_{0.77}$, $PbSe_{0.39}S_{0.61}$, $PbSe_{0.49}S_{0.51}$, $PbSe_{0.68}S_{0.32}$, and $PbSe_{0.90}S_{0.10}$. In all cases, approximate errors are <2.1%. From this and a comparison to their respective theoretical stoichiometries, it is evident that ternary NWs possess more selenium than expected. This deviation is pronounced in samples produced from selenium-rich precursor mixtures. However, these deviations never exceed 13.3% of the expected composition based on the introduced precursor stoichiometry.

The ICP-AES results can also be compared to the earlier ensemble EDXS stoichiometries in Table 1. It is apparent that differences exist between these measurements. Given that we have assumed a 1:1 metal-to-chalcogen (*i.e.*, S + Se) stoichiometry in our EDXS Cliff–Lorimer analysis (Supporting Information) to circumvent the S/Pb EDXS overlap, it is not surprising to find such differences between techniques. The conclusion is drawn tighter by the fact that both ICP-AES and EDXS results on binary PbSe/PbS NWs show slight nonstoichiometric metal/chalcogen mole ratios [EDXS: Pb/Se 54%/46%; ICP-AES: Pb/Se 51%/49%; Pb/S 54%/46%]. Samples always have a tendency to be lead rich. The ensemble EDXS data are therefore used as a first-order estimate of the NW composition.

As an added result from these ICP-AES measurements, we find the following synthetic yields for our ternary NW reactions: PbSe (36%), $PbSe_{0.23}S_{0.77}$ (28%), $PbSe_{0.39}S_{0.61}$ (42%), $PbSe_{0.49}S_{0.51}$ (38%), $PbSe_{0.68}S_{0.32}$ (32%), $PbSe_{0.90}S_{0.10}$ (44%), and PbS (17%). These yields are found from a detailed analysis described in the Supporting Information (Table S2).

A critical aspect in the controlled production of compositionally complex materials is the level of compositional homogeneity within a given wire. To evaluate this, we must go beyond ensemble EDXS and ICP-AES measurements. As a consequence, we have acquired single-wire EDXS spectra to better evaluate potential intrawire compositional fluctuations. This has entailed collecting EDXS line scans along the length of individual NWs with 10 separate EDXS spectra taken for each wire. The spacing of spectra was kept less than 200 nm to minimize specimen drift even though an automated TEM drift correction procedure was employed. Figure 7 shows a representative spectrum, where Figure 7a first illustrates a Z-contrast image of a small ternary $PbSe_{0.60}S_{0.40}$ NW bundle obtained through high-angle annular dark field (HAADF) scanning transmission electron microscopy. Figure 7b then illustrates one of 10 EDXS spectra acquired along a given wire's length as indicated by the solid white line in Figure 7a. The EDXS data show the presence of Pb and Se as well as the unavoidable overlap between the sulfur K and lead M lines. Attempts at radial scans were not successful, as the observed EDXS counts were too small to obtain good signal-to-noise ratios.

In total, 10 individual NWs from each of three different ternary $PbSe_xS_{1-x}$ ensembles were analyzed. By applying the same EDXS Cliff–Lorimer analysis used earlier to circumvent the sulfur/lead spectral overlap, intrawire compositions of $PbSe_{0.20}S_{0.80}$, $PbSe_{0.50}S_{0.50}$, and $PbSe_{0.60}S_{0.40}$ NWs were estimated. Table 2 shows resulting data taken from 30 individual wires, 10 wires from each ternary ensemble. The average composition,

TABLE 2. Average Composition of $PbSe_xS_{1-x}$ NWs Calculated from Single-Wire EDXS Line Scans

	$PbSe_{0.20}S_{0.80}$		$PbSe_{0.50}S_{0.50}$		$PbSe_{0.60}S_{0.40}$	
NW	x^a	$\pm\sigma^b$	x^a	$\pm\sigma^b$	x^a	$\pm\sigma^b$
1	0.13	0.03	0.59	0.10	0.69	0.07
2	0.16	0.03	0.59	0.08	0.66	0.07
3	0.15	0.04	0.45	0.06	0.66	0.08
4	0.17	0.05	0.53	0.08	0.62	0.04
5	0.16	0.06	0.43	0.13	0.60	0.09
6	0.15	0.05	0.41	0.11	0.63	0.06
7	0.14	0.03	0.72	0.10	0.74	0.10
8	0.16	0.03	0.52	0.08	0.68	0.08
9	0.13	0.03	0.54	0.08	0.69	0.14
10	0.15	0.04	0.39	0.05	0.73	0.07
average	0.15^c	0.04^d	0.52^c	0.13^d	0.67^c	0.09^d

[a,b] Average composition ($x \pm \sigma$) of each wire from 10 EDXS spectra taken along the wire's length. [c,d] Average composition ($x \pm \sigma$) calculated from 100 EDXS spectra (10 spectra for each of 10 wires investigated).

$x \pm \sigma$, is reported for each wire, from 10 EDXS spectra taken along the wire's length. For each ternary $PbSe_xS_{1-x}$ NW ensemble, the average composition, calculated from 100 EDXS spectra (10 spectra for each of 10 wires investigated), is also reported at the bottom of Table 2. A complete list can be found in the Supporting Information (Table S3). In each case, an examination shows that the average composition fluctuates 6.83 ± 0.03% about the introduced precursor stoichiometry. At most a 14% variation exists in this value. Half of the line scans give the exact input stoichiometry, and no sections of any wire lacked S, Se, or Pb. Furthermore, no compositional gradients, like those seen in $ZnSe_xTe_{1-x}$ NWs,[44] were observed.

Note that given the above-mentioned limitations of the EDXS analysis, these values are only approximate. What we wish to highlight is the compositional control achieved in the preparation of these wires. Specifically, Table 2 shows that despite slight compositional fluctuations, the use of single-source precursors leads to ternary alloys with relatively consistent metal/chalcogen compositions. This demonstrates the advantage of using single-source precursors in the growth of compositionally complex systems where finding separate metal and chalcogen precursors with appropriate reactivities/decomposition kinetics can be problematic.

In all of our studies, we have seen that the estimated chalcogen content of the ternary NWs differs slightly from the expected amount. We speculate that this may arise due to the different decomposition kinetics of $Pb((SeP^iPr_2)_2N)_2$ *versus* $Pb(S_2CNEt_2)_2$. Such a scenario is plausible given that, even in compositionally analogous single-source precursors, bond strengths can differ, leading to different decomposition kinetics. Supporting this, empirical observations suggest that $Pb((SeP^iPr_2)_2N)_2$ decomposes more readily than $Pb(S_2CNEt_2)_2$ since it is noticeably more temperature sensitive. However, the actual mechanism for single-source precursor decomposition is not known. Alternatively, small compositional deviations may arise due to the different solubilities of S and Se in Bi or to different PbS *versus* PbSe growth rates. Despite these ambiguities, Tables 1 and 2 along with all of the available data indicate that ternary lead chalcogenide alloys, fully spanning the PbS/PbSe compositional gap, can be made. The current study therefore reports the growth of compositionally tunable $PbSe_xS_{1-x}$ NWs from single-source precursors.

Finally, we investigated the optical properties of the synthesized binary and ternary NWs. The extinction spectra of nanowire films drop-cast onto microscope coverslips from chloroform suspensions were taken on a JASCO V-670 UV–vis–NIR spectrophotometer. All acquired spectra currently lack well-defined band-edge peaks (Supporting Information, Figure S7). This could be due to the residual size distribution of each NW ensemble and/or the masking effect of passivating ligand vibrational transitions. In the latter case, ligand-exchanging TOPO for pyridine or oleic acid led to no significant differences. Spectra of NWs suspended in tetrachloromethane, tetrachloroethylene, and chloroform also show no band-edge features. Thus, at this point, we are unable to report in detail on the optical properties of the synthesized binary and ternary NWs.

CONCLUSIONS

We have successfully prepared high-quality $PbSe_xS_{1-x}$ (x = 0.23, 0.39, 0.49, 0.68, and 0.90) NWs as well as their binary PbSe and PbS analogues through the use of $Pb(S_2CNEt_2)_2$ and $Pb((SeP^iPr_2)_2N)_2$ single-source precursors. Detailed XRD studies confirm the ternary nature of the wires and reveal composition-dependent lattice constants tunable between the corresponding PbSe and PbS limits. Additional ensemble and single-NW EDXS measurements as well as ensemble ICP-AES measurements reveal stoichiometries that deviate slightly from expected metal/chalcogen concentrations. Complementary, single-wire EDXS line profile scans likewise reveal slight intrawire compositional inhomogeneities. These variations never exceed 14% (average 6.83 ± 0.03%) of the expected stoichiometry and along with the ensemble EDXS/ICP-AES results indicate the high degree of compositional control achieved with the current synthesis. The successful growth of ternary $PbSe_xS_{1-x}$ NWs demonstrates the usefulness of single-source precursors in producing compositionally complex systems

and opens the door to alloyed nanostructures that can be further explored for their size- and composition-dependent optical, electrical, and thermal properties.

MATERIALS AND METHODS

Materials. Chlorodiisopropylphosphine ($^{i}Pr_2PCl$, 96%), 1,1,1,3,3,3-hexamethyldisilazane ($NH(SiMe_3)_2$, 98%), sodium methoxide (pure, anhydrous powder), selenium powder (99.5+%, 200 mesh), bismuth(III) chloride (98+%), and sodium diethyldithiocarbamate trihydrate ($NaS_2CNEt_2 \cdot 3H_2O$, ACS grade) were purchased from Acros Organics. Trioctylphosphine oxide (99%) and lead(II) selenide powder (99.99%, PURATREM) were purchased from Strem Chemicals. Trioctylphosphine (90%) and lead nitrate (99.999%) were purchased from Aldrich. Lead chloride (99%) was purchased from Fisher Scientific. Lead(II) sulfide powder (99.995%, metal basis) was purchased from Alfa Aesar. Methanol, acetone, and toluene were purchased from VWR. Anhydrous methanol was obtained by successively distilling it with a rectification column, passing it slowly over a column of dry molecular sieves, and then distilling it over metallic sodium.[62] Lead (2% HNO_3, 1000 mg/L) and selenium (2% HNO_3, 1000 mg/L) ICP standards were purchased from Spex CertiPrep and were used as received. A sulfur (2% HNO_3, 999.73 ppm) ICP standard was prepared from ammonium sulfate (Mallinckrodt, Inc.) and 2% HNO_3. HNO_3 (69.4% v/v) was purchased from Fisher Scientific and used as received. HCl (36.5−38.0% min, v/v) was purchased from VWR and used as received. Bismuth catalyst solution was prepared fresh prior to each NW synthesis by dissolving 0.0126 mg (40 μmol) of $BiCl_3$ in 20 mL of acetone to give a 2 mM solution. On occasion, 5 mL of this solution was diluted to 1 mM. Aliquots of the $BiCl_3$ solution were then added to the injection solution. All chemicals were used as received, unless otherwise stated. The molecular structures of the $Pb((SeP^{i}Pr_2)_2N)_2$ and $Pb(S_2CNEt_2)_2$ single-source precursors are shown in the Supporting Information (Figure S8).

Synthesis of $Pb((SeP^{i}Pr_2)_2N)_2$. The synthesis of $Pb((SeP^{i}Pr_2)_2N)_2$ was carried out using a two-step, modified literature procedure under nitrogen.[63,64] The first step involved preparing the intermediate, bis(diisopropylselenophosphino)amine, $NH(SeP^{i}Pr_2)_2$.[64] In a typical preparation, a solution of $^{i}Pr_2PCl$ (5.00 g, 32.8 mmol) in toluene (100 mL) was added dropwise to a stirring solution of $NH(SiMe_3)_2$ (3.50 mL, 16.5 mmol) in toluene (50 mL) at 50 °C over the course of 30 min. The reaction was then continued for 3 h at 50 °C and was thereafter cooled to room temperature. Selenium powder (2.53 g, 32.0 mmol) was then added followed by a 6 h reflux. During this step, the reaction mixture turned yellow-orange. Once complete, it was cooled to room temperature, and the solvent was removed using a rotary evaporator. An oily yellow-orange mixture resulted and was washed with hexane. This involved centrifuging the suspension and discarding the supernatant. The hexane washing step was continued until the supernatant became colorless. Any unreacted selenium was removed by dissolving the crude intermediate, $NH(SeP^{i}Pr_2)_2$, in chloroform and centrifuging off a black precipitate. Subsequent recrystallization of the product was done by dissolving it in chloroform (~5 mL) and reprecipitating it with hexane (~20 mL). The desired off-white $NH(SeP^{i}Pr_2)_2$ intermediate was recovered.

The second step of the synthesis entailed adding sodium methoxide (0.175 g, 3.2 mmol) to a solution of $NH(SeP^{i}Pr_2)_2$ (1.32 g, 3.2 mmol) in anhydrous methanol (40 mL). The resulting mixture was then stirred at room temperature for 10 min. $PbCl_2$ (0.9185 g, 3.3 mmol) was added to the reaction mixture and was stirred continuously at room temperature for 2 h. A yellow product was recovered by centrifugation and was washed with methanol (20 mL) to remove any excess reagent. The product was then recrystallized by dissolving it in a minimal amount of chloroform (<5 mL) and reprecipitating it with anhydrous methanol (~20 mL). ESI-MS: 1022.99 ($M + nH$). ^{1}H NMR (400 MHz, $CDCl_3$): δ ppm 2.20 (m, 8 H), 1.22 (m, 48 H). ^{31}P NMR (MHz, $CDCl_3$): δ ppm 56.63 (s, 1 P). ^{13}C NMR (MHz, $CDCl_3$): δ ppm 33.18, 17.18. Anal. Calcd for $PbC_{24}H_{56}N_2P_4Se_4$: C, 28.27; H, 5.54; N, 2.75. Found: C, 28.69; H, 5.98; N, 2.79.

Synthesis of $Pb(S_2CNEt_2)_2$. This compound was obtained as a white precipitate by mixing aqueous solutions of $NaS_2CNEt_2 \cdot 3H_2O$ and $Pb(NO_3)_2$ in a 2:1 molar ratio. The product was then recrystallized from boiling toluene to give white crystals. ESI-MS: 505.03 ($M + nH$). ^{1}H NMR (400 MHz, $CDCl_3$): δ ppm 3.79 (m, 8 H), 1.33 (t, 12 H). ^{13}C NMR (400 MHz, $CDCl_3$): δ ppm 47.49, 12.47. Anal. Calcd. for $PbC_{10}H_{20}N_2S_4$: C, 23.8; H, 5.56; N, 4.00. Found: C, 23.5; H, 5.70; N, 4.10.

Synthesis of PbSe NWs. In a typical synthesis, TOPO (4 g, 10.3 mmol) was dried and degassed at 100 °C for 2 h in a three-neck round-bottom flask connected to a Schlenk line. The reaction vessel was then backfilled with N_2, and the temperature was raised to 210 °C. In tandem, $Pb((SeP^{i}Pr_2)_2N)_2$ (20 mg, 19.6 μmol) was added to TOP (0.3 mL, 1 mmol) in a small vial. The mixture was gently heated on a hot plate while shaking it until the single-source precursor dissolved completely to yield a yellow solution. The lead precursor was then cooled to room temperature and was mixed with a 1 mM $BiCl_3$ solution (25 μL, 25 nmol) in a syringe. When the temperature of the TOPO stabilized at 210 °C, this precursor solution was injected into the three-neck flask. An immediate color change to black resulted. Following injection, the reaction mixture was held at ~210 °C for 2 min. Afterward, it was cooled to 70 °C, whereupon toluene (~15 mL) was added to prevent TOPO from solidifying. Resulting NWs were precipitated using excess methanol (~15 mL) and were recovered by centrifuging the suspension, discarding the supernatant. A toluene/methanol mixture (1:1 by volume) was subsequently added to wash the NWs of excess surfactant. The suspension was again centrifuged, and the product was recovered. This washing procedure was repeated at least two more times, whereupon the recovered NWs were stored in toluene.

Synthesis of PbS NWs. PbS NWs were synthesized according to a modified literature procedure.[24] Typically, TOPO (2 g, 5.2 mmol) was dried and degassed in a three-neck flask connected to a Schlenck line at 100 °C for 1 h. The reaction vessel was then backfilled with N_2, and the temperature was increased to 210 °C. $Pb(S_2CNEt_2)_2$ (10 mg, 20 μmol) was added to TOP (0.5 mL, 1.12 mmol) in a glass vial and was dissolved by gently heating it with a heat gun. At the same time, TOP (0.1 mL, 0.22 mmol) and 25 μL (25 nmol) of a 1 mM $BiCl_3$ solution were combined in a syringe. The Pb precursor solution was then added to the same syringe while hot. The resulting injection solution was rapidly introduced into TOPO at 210 °C. The mixture immediately turned black and was held at this temperature for 2 min. Thereafter, it was cooled to 70 °C, and toluene (~5 mL) was added to prevent TOPO from solidifying. Resulting NWs were purified as described above and were subsequently stored in toluene.

Synthesis of $PbSe_xS_{1-x}$ NWs. In a typical synthesis of $PbSe_{0.5}S_{0.5}$ NWs, TOPO (4 g, 10.3 mmol) was dried and degassed at 100 °C for 2 h in a three-neck flask connected to a Schlenk line. The vessel was then backfilled with N_2 and the temperature was raised to 210 °C. TOP (0.2 mL, 0.6 mmol) was added to $Pb((SeP^{i}Pr_2)_2N)_2$ (20 mg, 20 μmol) in a glass vial. The precursor was dissolved by gently heating it on a hot plate. A yellow solution resulted. It was subsequently cooled to room temperature. Then 2 mM $BiCl_3$ (25 μL, 50 nmol) was added, and the resulting mixture was loaded into a syringe. In tandem, $Pb(S_2CNEt_2)_2$ (10 mg, 20 μmol) was mixed with TOP (0.5 mL, 15 mmol) in a separate glass vial followed by gentle heating with a heat gun to dissolve it. This hot solution was immediately added to the $Pb((SeP^{i}Pr_2)_2N)_2$-containing syringe and was injected into the three-neck flask at 210 °C. The mixture immediately turned black and was held at this temperature for 2 min. It was

subsequently cooled to 70 °C, whereupon toluene (~15 mL) was introduced to prevent TOPO from solidifying. Resulting NWs were purified as described above and were stored in toluene. To change the $PbSe_xS_{1-x}$ NW composition, the single-source precursor mole ratio, $Pb((SeP^iPr_2)_2N)_2$:-$Pb(S_2CNEt_2)_2$, was systematically varied as follows: 4:1, 1.5:1, 1:1, 1:1.5, and 1:4. All other aspects of the preparation were kept the same.

Structural and Spectroscopic Characterization. ^1H, ^{13}C, and ^{31}P nuclear magnetic resonance (NMR) spectra of the single-source precursors were measured on a Bruker 400 MHz spectrometer (Supporting Information Figures S9–S13). An internal tetramethylsilane (TMS) reference was used. Elemental analysis of the single-source precursors was performed on a Costech ECS 1040 elemental analyzer and was subsequently confirmed with a Carlo Erba EA1108 elemental analyzer equipped with a Finnigan Delta Plus stable isotope mass spectrometer (Supporting Information Figures S14, S15). TEM experiments entailed dropping dilute suspensions of NWs onto 200 mesh ultrathin carbon TEM grids (Ladd Research). Samples were previewed using a JEOL 100SX instrument. Subsequent low- and high-resolution TEM micrographs were taken with a JEOL 2010 TEM operating at 200 kV as well as with a Titan 80-300 (FEI) operating at 300 kV. Elemental analyses of NW ensembles were conducted using an EDXS attachment (Thermo Scientific) to the JEOL 2010 microscope with commercial PbSe and PbS powders as standards. The compositions of all NWs, the synthesized single-source precursors, and commercially available PbSe and PbS standards were independently confirmed by elemental analysis using inductively coupled plasma atomic emission spectroscopy with a Perkin-Elmer Optima 3300XL. SAED images, single-wire EDXS line scans, and HAADF-STEM images were acquired using a Titan 80-300 TEM. X-ray diffraction patterns were taken with a Bruker D8 Discover diffractometer (Cu Kα source).

ICP-AES Procedure. Synthesized NWs were separated from their solvent by centrifugation and were dried overnight under low heat. Dried NWs were dissolved in ~1.5 mL of a 1:2 HNO_3/HCl mixture, prepared from commercially available concentrated acids. NW solutions were diluted to a concentration of ~5% by volume (for both HNO_3 and HCl) by adding 5.5 mL of distilled water. An ICP-AES calibration curve was then built using standard solutions containing lead, selenium, and sulfur with known ppm concentrations in 5% HNO_3/HCl. Standard solutions were analyzed by ICP-AES, with the calibration curve (emission intensity *versus* concentration) for each element built automatically by the analysis software. The following wavelengths gave the best signal-to-noise ratios as well as the lowest relative standard deviations. They were therefore used in subsequent ICP-AES analyses: Pb (220.353 nm), Se (196.026 nm), and S (180.669 nm). Prepared NW solutions were then analyzed, and their ppm concentrations were automatically calculated from the calibration curve. Each measurement was carried out in triplicate with the average reported (relative standard deviations never exceeded 1.2%). Finally, associated molar concentrations were calculated for each element and were reported as molar ratios of Se to S for the ternary NWs and Pb to Se (S) for the binary NWs.

Conflict of Interest: The authors declare no competing financial interest.

Acknowledgment. This work was supported by the Notre Dame Strategic Research Initiative. M.K. also thanks the National Science Foundation CAREER program (CHE-0547784) and the Notre Dame Radiation Laboratory/Department of Energy, Office of Basic Energy Sciences for partial financial support and for use of their facilities. The authors thank the Notre Dame Center for Environmental Science and Technology for use of their equipment. We thank Felix Vietmeyer and Galyna Krylova for assistance with the ICP-AES analysis. We also thank Liubov Shapoval from the Fulbright Foreign Student Program and Dr. Vladimir Plashnitsa for assistance with TEM imaging, NW sizing, and useful discussions.

Supporting Information Available: Table of synthetic conditions and results for PbSe and PbS NWs. Additional TEM images of PbSe and PbS NWs. Plot of XRD peak positions *versus* ternary NW composition. Bowing deviation from Vegard's law. Ensemble PbSe NW EDXS spectrum. Cliff–Lorimer analysis. Synthetic yields from ICP-AES measurements. Table of single-NW EDXS line scan data. Extinction spectra of the synthesized NWs. Molecular structures of the single-source precursors. Structural characterization (^1H NMR, ^{13}C NMR, ^{31}P NMR, and ESI-MS spectra) of single-source precursors. This material is available free of charge via the Internet at http://pubs.acs.org.

REFERENCES AND NOTES

1. Masek, J.; Maissen, C.; Zogg, H.; Platz, W.; Riedel, H.; Königer, M.; Lambrecht, A.; Tacke, M. Photovoltaic Lead-Chalcogenide IR-Sensor Arrays on Si for Thermal Imaging Applications. *Nucl. Instrum. Methods A* **1990**, *288*, 104–109.
2. Zogg, H.; Alchalabi, K.; Zimin, D.; Kellermann, K.; Buttler, W. Two-Dimensional Monolithic Lead Chalcogenide Infrared Sensor Array on Silicon Read-Out Chip. *Nucl. Instrum. Methods A* **2003**, *512*, 440–444.
3. Ma, W.; Luther, J. M.; Zheng, H.; Wu, Y.; Alivisatos, A. P. Photovoltaic Devices Employing Ternary PbS_xSe_{1-x} Nanocrystals. *Nano Lett.* **2009**, *9*, 1699–1703.
4. Klem, E. J. D.; MacNeil, D. D.; Levina, L.; Sargent, E. H. Solution Processed Photovoltaic Devices with 2% Infrared Monochromatic Power Conversion Efficiency: Performance Optimization and Oxide Formation. *Adv. Mater.* **2008**, *20*, 3433–3439.
5. Marchetti, S.; Giorgi, M.; Lazzari, C.; Palleschi, V.; Simili, R. Fast Detection in the Near and Medium Infrared by Means of Transverse Dember Effect in Anisotropic PbS and PbSe Films. *Infrared Phys.* **1993**, *34*, 137–141.
6. Liu, X.; Zhang, M. Studies on PbS and PbSe Detectors for IR System. *Int. J. Infrared Millimeter Waves* **2000**, *21*, 1697–1701.
7. Liang, W.; Rabin, O.; Hochbaum, A. I.; Fardy, M.; Zhang, M.; Yang, P. Thermoelectric Properties of p-Type PbSe Nanowires. *Nano Res.* **2009**, *2*, 394–399.
8. Fardy, M.; Hochbaum, A. I.; Goldberger, J.; Zhang, M. M.; Yang, P. Synthesis and Thermoelectric Characterization of Lead Chalcogenide Nanowires. *Adv. Mater.* **2007**, *19*, 3047–3051.
9. Kang, I.; Wise, F. W. Electronic Structure and Optical Properties of PbS and PbSe Quantum Dots. *J. Opt. Soc. Am. B* **1997**, *14*, 1632–1646.
10. Urban, J. J.; Talapin, D. V.; Shevchenko, E. V.; Murray, C. B. Self-Assembly of PbTe Quantum Dots into Nanocrystal Superlattices and Glassy Film. *J. Am. Chem. Soc.* **2006**, *128*, 3248–3255.
11. Wise, F. W. Lead Salt Quantum Dots: The Limit of Strong Quantum Confinement. *Acc. Chem. Res.* **2000**, *33*, 773–780.
12. Schaller, R. D.; Klimov, V. I. High Efficiency Carrier Multiplication in PbSe Nanocrystals: Implications for Solar Energy Conversion. *Phys. Rev. Lett.* **2004**, *92*, 186601.
13. Ellingson, R. J.; Beard, M. C.; Johnson, J. C.; Yu, P.; Micic, O. I.; Nozik, A. J.; Shabaev, A.; Efros, A. L. Highly Efficient Multiple Exciton Generation in Colloidal PbSe and PbS Quantum Dots. *Nano Lett.* **2005**, *5*, 865–871.
14. Giblin, J.; Kuno, M. Nanostructure Absorption: A Comparative Study of Nanowire and Colloidal Quantum Dot Absorption Cross Sections. *J. Phys. Chem. Lett.* **2010**, *1*, 3340–3348.
15. Singh, A.; Li, X.; Protasenko, V.; Galantai, G.; Kuno, M.; Xing, H.; Jena, D. Polarization-Sensitive Nanowire Photodetectors Based on Solution-Synthesized CdSe Quantum-Wire Solids. *Nano Lett.* **2007**, *7*, 2999–3006.
16. Yu, Y.; Protasenko, V; Jena, D; Xing, H. G; Kuno, M. Photocurrent Polarization Anisotropy of Randomly Oriented Nanowire Networks. *Nano Lett.* **2008**, *8*, 1352–1357.
17. Bierman, M. J.; Lau, Y. K. A.; Jin, S. Hyperbranched PbS and PbSe Nanowires and the Effect of Hydrogen Gas on their Synthesis. *Nano Lett.* **2007**, *7*, 2907–2912.

18. Ge, J.-P.; Wang, J.; Zhang, H. X.; Wang, X.; Peng, Q.; Li, Y.-D. Orthogonal PbS Nanowire Arrays and Networks and their Raman Scattering Behavior. *Chem.—Eur. J.* **2005**, *11*, 1889–1894.
19. Lau, Y. K. A.; Chernak, D. J.; Bierman, M. J.; Jin, S. Formation of PbS Nanowire Pine Trees Driven by Screw Dislocations. *J. Am. Chem. Soc.* **2009**, *131*, 16461–16471.
20. Hujdic, J. E.; Taggart, D. K.; Kung, S.-C.; Menke, E. J. Lead Selenide Nanowires Prepared by Lithographically Patterned Nanowire Electrodeposition. *J. Phys. Chem. Lett.* **2010**, *1*, 1055–1059.
21. Zhang, F.; Wong, S. S. Controlled Synthesis of Semiconductor Metal Sulfide Nanowires. *Chem. Mater.* **2009**, *21*, 4541–4554.
22. Lau, Y. K. A.; Chernak, D. J.; Bierman, M. J.; Jin, S. Epitaxial Growth of Hierarchical PbS Nanowires. *J. Mater. Chem.* **2009**, *19*, 934–940.
23. Yong, K.-T.; Sahoo, Y.; Choudhury, K. R.; Swihart, M. T.; Minter, J. R.; Prasad, P. N. Control of the Morphology and Size of PbS Nanowires Using Gold Nanoparticles. *Chem. Mater.* **2006**, *18*, 5965–5972.
24. Sun, J.; Buhro, W. E. The Use of Single-Source Precursors for the Solution-Liquid-Solid Growth of Metal Sulfide Semiconductor Nanowires. *Angew. Chem., Int. Ed.* **2008**, *47*, 3215–3218.
25. Hull, K. L.; Grebinski, J. W.; Kosel, T. H.; Kuno, M. Induced Branching in Confined PbSe Nanowires. *Chem. Mater.* **2005**, *17*, 4416–4425.
26. Xu, F.; Ma, X.; Gerlein, L. F.; Cloutier, S. G. Designing and Building Nanowires: Directed Nanocrystal Self-Assembly into Radically Branched and Zigzag PbS Nanowires. *Nanotechnology* **2011**, *22*, 265604.
27. Cho, K.-S.; Talapin, D. V.; Gaschler, W.; Murray, C. B. Designing PbSe Nanowires and Nanorings Through Oriented Attachment of Nanoparticles. *J. Am. Chem. Soc.* **2005**, *127*, 7140–7147.
28. Wang, Z.; Zhao, B.; Zhang, F.; Wao, W.; Qian, G.; Fan, X. Novel Single-Crystal PbS Nanowires Directed by [200]. *Mater. Lett.* **2007**, *61*, 3733–3735.
29. Foos, E. E.; Zega, T. J.; Tischler, J. G.; Stroud, R. M.; Boercker, J. E. Synthesis of PbSe Nanowires: The Impact of Alkylphosphonic Acid Addition. *J. Mater. Chem.* **2011**, *21*, 2616–2623.
30. Trentler, T. J.; Hickman, K. M.; Goel, S. C.; Viano, A. M.; Gibbons, P. C.; Buhro, W. E. Solution-Liquid-Solid Growth of Crystalline III-V Semiconductors: An Analogy to Vapor-Liquid-Solid Growth. *Science* **1995**, *270*, 1791–1794.
31. Wang, F.; Dong, A.; Sun, J.; Tang, R.; Yu, H.; Buhro, W. E. Solution-Liquid-Solid Growth of Semiconductor Nanowires. *Inorg. Chem.* **2006**, *45*, 7511–7521.
32. Malik, M. A.; Afzaal, M.; O'Brien, P. Precursor Chemistry for Main Group Elements in Semiconducting Materials. *Chem. Rev.* **2010**, *110*, 4417–4446.
33. Wooten, A. F.; Werder, D. J.; Williams, D. J.; Casson, J. L.; Hollingsworth, J. A. Solution-Liquid-Solid Growth of Ternary Cu-In-Se Semiconductor Nanowires from Multiple- and Single-Source Precursors. *J. Am. Chem. Soc.* **2009**, *131*, 16177–16188.
34. Wang, Z.; Li, Z.; Kornowski, A.; Ma, X.; Myalitsin, A.; Mews, A. Solution-Liquid-Solid Synthesis of Semiconductor Nanowires using Clusters as Single-Source Precursors. *Small* **2011**, *7*, 2464–2468.
35. Akhtar, J.; Afzaal, M.; Banski, M.; Podhorodecki, A.; Syperek, M.; Misiewicz, J.; Bangert, U.; Hardman, S. J. O.; Graham, D. M.; Flavell, W. R.; *et al.* Controlled Synthesis of Tuned Band Gap Nanodimensional Alloys of PbS_xSe_{1-x}. *J. Am. Chem. Soc.* **2011**, *133*, 5602–5609.
36. Zhong, X.; Feng, Y.; Knoll, W.; Han, M. Alloyed $Zn_xCd_{1-x}S$ Nanocrystals with Highly Narrow Luminescence Spectra Width. *J. Am. Chem. Soc.* **2003**, *125*, 13559–13563.
37. Zhong, X.; Han, M.; Dong, Z.; White, T. J.; Knoll, W. Composition-Tunable $Zn_xCd_{1-x}Se$ Nanocrystals with High Luminescence and Stability. *J. Am. Chem. Soc.* **2003**, *125*, 8589–8594.
38. Swafford, L. A.; Weigand, L. A.; Bowers, M. J.; McBride, J. R.; Rapaport, J. L.; Watt, T. L.; Dixit, S. K.; Feldman, L. C.; Rosenthal, S. J. Homogenously Alloyed CdS_xSe_{1-x} Nanocrystals: Synthesis, Characterization, and Composition/Size-Dependent Band Gap. *J. Am. Chem. Soc.* **2006**, *128*, 12299–12306.
39. Bailey, R. E.; Nie, S. Alloyed Semiconductor Quantum Dots: Tuning the Optical Properties without Changing the Particle Size. *J. Am. Chem. Soc.* **2003**, *125*, 7100–7106.
40. Smith, D. K.; Luther, J. E.; Semonin, O. E.; Nozik, A. J.; Beard, M. C. Tuning the Synthesis of Ternary Lead Chalcogenide Quantum Dots by Balancing Precursor Reactivity. *ACS Nano* **2011**, *5*, 183–190.
41. Xu, J.; Tang, Y.-B.; Chen, X.; Luan, C.-Y.; Zhang, W.-F.; Zapien, J. A.; Zhang, W.-J.; Kwong, H.-L.; Meng, X.-M.; Lee, S.-T.; *et al.* Synthesis of Homogenously Alloyed $Cu_{2-x}S_ySe_{1-y}$ Nanowire Bundles with Tunable Compositions and Band Gaps. *Adv. Funct. Mater.* **2010**, *20*, 4190–4195.
42. Kuykendall, T.; Ulrich, P.; Aloni, S.; Yang, P. Complete Composition Tunability of InGaN Nanowires using a Combinatorial Approach. *Nat. Mater.* **2007**, *6*, 951–956.
43. Wang, M.; Fei, G. T.; Zhang, Y. G.; Kong, M. G.; Zhang, L. D. Tunable and Predetermined Band Gap Emissions in Alloyed ZnS_xSe_{1-x} Nanowires. *Adv. Mater.* **2007**, *19*, 4491–4494.
44. Dong, A.; Wang, F.; Daulton, T. L.; Buhro, W. E. Solution-Liquid-Solid (SLS) Growth of ZnSe-ZnTe Quantum Wires Having Axial Heterojuctions. *Nano Lett.* **2007**, *7*, 1308–1313.
45. Mokari, T.; Habas, S. E.; Zhang, M.; Yang, P. Synthesis of Lead Chalcogenide Alloy and Core-Shell Nanowires. *Angew. Chem., Int. Ed.* **2008**, *47*, 5605–5608.
46. Grebinski, J. W.; Richter, K. L.; Zhang, J.; Kosel, T. H.; Kuno, M. Synthesis and Characterization of Au/Bi Core/Shell Nanocrsytals: A Precursor toward II-VI Nanowires. *J. Phys. Chem. B* **2004**, *108*, 9745–9751.
47. Wang, F.; Buhro, W. E. An Easy Shortcut Synthesis of Size-Controlled Bismuth Nanoparticles and their Use in the SLS Growth of High Quality Colloidal Cadmium Selenide Quantum Wires. *Small* **2010**, *6*, 573–581.
48. Grebinski, J. W.; Hull, K. L.; Zhang, J.; Kosel, T. H.; Kuno, M. Solution-Based Straight and Branched CdSe Nanowires. *Chem. Mater.* **2004**, *16*, 5260–5272.
49. Kuno, M; Ahmad, O.; Protasenko, V.; Bacinello, D.; Kosel, T. H. Solution-Based Straight and Branched CdTe Nanowires. *Chem. Mater.* **2006**, *18*, 5722–5732.
50. Puthussery, J.; Kosel, T. H.; Kuno, M. Facile Synthesis and Size Control of II-VI Nanowires using Bismuth Salts. *Small* **2009**, *5*, 1112–1116.
51. Fultz, B.; Howe, J. *Transmission Electron Microscopy and Diffractometry of Materials*, 2nd ed.; Springer: New York, 2002.
52. Kuno, M. An Overview of Solution-Based Semiconductor Nanowires: Synthesis and Optical Studies. *Phys. Chem. Chem. Phys.* **2008**, *10*, 620–639.
53. Puthussery, J.; Lan, A.; Kosel, T. H.; Kuno, M. Band-Filling of Solution-Synthesized CdS Nanowires. *ACS Nano* **2008**, *2*, 357–367.
54. Singh, J. *Electronic and Optoelectronic Properties of Semiconductor Structures*; Cambridge University Press: Cambridge, UK, 2003.
55. Boukhris, N.; Meradji, H.; Ghemid, S.; Drablia, S.; Hassan, F. E. H. *Ab Initio* Study of the Structural, Electronic and Thermodynamic Properties of $PbSe_{1-x}S_x$, $PbSe_{1-x}Te_x$ and $PbS_{1-x}Te_x$ Ternary Alloys. *Phys. Scr.* **2011**, *83*, 065701.
56. Bernard, J. E.; Zunger, A. Electronic Structure of ZnS, ZnSe, ZnTe, and their Pseudobinary Alloys. *Phys. Rev. B* **1987**, *36*, 3199–3228.
57. Wei, S.-H.; Zhang, S. B.; Zunger, A. First-Principles Calculation of Band Offsets, Optical Bowings, and Defects in CdS, CdSe, CdTe, and their Alloys. *J. Appl. Phys.* **2000**, *87*, 1304–1311.
58. Smith, A. M.; Mohs, A. M.; Nie, S. Tuning the Optical and Electronic Properties of Colloidal Nanocrystals by Lattice Strain. *Nat. Nanotechnol.* **2009**, *4*, 56–63.

59. Meulenberg, R. W.; Jennings, T.; Strouse, G. F. Compressive and Tensile Stress in Colloidal CdSe Semiconductor Quantum Dots. *Phys. Rev. B* **2004**, *70*, 235311.
60. Zhou, D; Usher, B. F. Deviation of the AlGaAs Lattice Constant from Vegard's Law. *J. Phys. D: Appl. Phys.* **2001**, *34*, 1461–1465.
61. Williams, D. B.; Carter, C. B. *Transmission Electron Microscopy*; Plenum Press: New York, 1996.
62. Marcus, Y.; Glikberg, S. Recommended Methods for the Purification of Solvents and Tests for Impurities: Methanol and Ethanol. *Pure Appl. Chem.* **1985**, *57*, 855–864.
63. Afzaal, M.; Ellwoood, K.; Pickett, N. L.; O'Brien, P.; Raftery, J.; Waters, J. Growth of Lead Chalcogenide Thin Films Using Single-Source Precursors. *J. Mater. Chem.* **2004**, *14*, 1310–1315.
64. Cupertino, D.; Birdsall, D. J.; Slawin, A. M. Z.; Woollins, J. D. The Preparation and Coordination Chemistry of $^{i}Pr_2P$-(E)NHP(E′)$^{i}Pr_2$ (E, E′ = Se; E = Se, E′ = S; E = S, E′ = O; E, E′ = O). *Inorg. Chim. Acta* **1999**, *290*, 1–7.